Crystal structures and characterization of two divalent metal selenates templated by dabco, (C6H14N2)[MII(H2O)6](SeO4)2 (MII: NiII, ZnII)

Nouha Loulou Nkhili, Walid Rekik, Houcine Naïli, Tahar Mhiri, Thierry Bataille

Arabian Journal of Chemistry (2017) **10**, S2509–S2517

King Saud University

Arabian Journal of Chemistry

www.ksu.edu.sa
www.sciencedirect.com

ORIGINAL ARTICLE

Crystal structures and characterization of two divalent metal selenates templated by dabco, $(C_6H_{14}N_2)[M^{II}(H_2O)_6](SeO_4)_2$ (M^{II}: Ni^{II}, Zn^{II})

Nouha Loulou Nkhili [a], Walid Rekik [a,*], Houcine Naïli [a], Tahar Mhiri [a], Thierry Bataille [b]

[a] *Laboratoire physico-chimie de l'état solide, Département de chimie, Faculté des Sciences de Sfax, Université de Sfax, BP 1171, 3000 Sfax, Tunisia*
[b] *Sciences Chimiques de Rennes (CNRS, UMR 6226), Université de Rennes 1, Avenue du Général Leclerc, 35042 Rennes Cedex, France*

Received 8 December 2012; accepted 12 September 2013
Available online 18 September 2013

KEYWORDS

Hybrid compounds;
Supramolecular;
Crystal structure;
Thermal decomposition;
Magnetic properties

Abstract Two new organic–inorganic hybrid materials have been synthesized and crystallographically characterized. Both compounds, $(C_6H_{14}N_2)[Ni(H_2O)_6](SeO_4)_2$ **(I)** and $(C_6H_{14}N_2)[Zn(H_2O)_6](SeO_4)_2$ **(II)**, crystallize isotypically in the monoclinic system, space group $P2_1/c$, with the following unit cell parameters: $a = 12.4045(3)$, $b = 11.9360(3)$, $c = 12.8366(3)$ Å, $\beta = 108.518(2)°$, $V = 1802.18(8)$ Å^3, $Z = 4$ for compound **(I)** and $a = 12.7839(2)$, $b = 11.9153(4)$, $c = 12.3814(2)$ Å, $\beta = 108.264(5)°$, $V = 1790.97(7)$ Å^3, $Z = 4$ for the zinc related phase. Their supramolecular structure consists of metallic cation octahedrally coordinated by six water molecules $[M^{II}(H_2O)_6]^{2+}$, selenate anions $(SeO_4)^{2-}$ and dabcodiium cation $(C_6H_{14}N_2)^{2+}$ linked together via two types of hydrogen bonds, Ow–H...O and N–H...O only. The thermal decomposition of these supramolecular compounds takes place in several steps leading to the formation of metal oxide. The magnetic measurements show that the nickel based compound is predominantly paramagnetic with weak antiferromagnetic interactions at low temperature.

1. Introduction

During the past few years, the design and the synthesis of the organic–inorganic hybrid materials have been of a great research interest due to their novel structural topologies and potential applications in the fields of catalysis and biochemistry (Hagrman et al., 1999; Cheetham, 1999; Férey, 2001; Soghomonian et al., 1993; Finn and Zubieta, 2000). We note that the organic–inorganic hybrid materials containing uranyl-based in

* Corresponding author. Tel.: +216 97 34 11 85; fax: +216 74 274 437.
E-mail address: w_rekik@alinto.com (W. Rekik).
Peer review under responsibility of King Saud University.

Production and hosting by Elsevier

http://dx.doi.org/10.1016/j.arabjc.2013.09.019
1878-5352

organic units were previously investigated (Krivovichev et al., 2005a,b, 2007; Borkowski and Cahill, 2006; Doran et al., 2003, 2005, 2004; Frisch and Cahill, 2007; Grechishnikova et al., 2006; Knope and Cahill, 2007; Norquist et al., 2005a,b, 2003; Ok et al., 2006; Ok and O'Hare, 2007; Wang et al., 2004; Yu et al., 2004). Recently, Krivovichev et al. (2007) examined the application of the charge-density matching principle to uranyl selenate organic–inorganic hybrids. We note also that a previous work of synthesis and characterization of metal sulfates templated by amines, leading to many important physical properties, has been realized in our laboratory (Rekik et al., 2006a,b, 2007, 2009, 2005, 2009; Naïli et al., 2006; Yahyaoui et al., 2007). This type of compounds has provided supramolecular structures and adopts similarities with the well-known Tutton's salts family (Maslen et al., 1988). However, an examination of the literature shows that a few hybrid selenate-containing transition metals have been reported (Ling et al., 2009; Feng et al., 2007, 2004; Zhang et al., 2009; Pasha and Choudhury, 2003). In the course of our search to extend this family of hybrid materials, two new compounds using 1,4-diaza-bicyclo[2.2.2]octane (dabco) as a template, selenate groups and transition metals have been synthesized. In this paper, we report the chemical preparation, the structural study, the infrared spectroscopy analysis, the magnetic measurements and the thermal behavior of the two compounds $(C_6H_{14}N_2)[M^{II}(H_2O)_6](SeO_4)_2$ ($M^{II} = Ni^{2+}$ (**I**) and Zn^{2+} (**II**)).

2. Experimental

2.1. Chemical preparation

Single crystals of the two compounds $(C_6H_{14}N_2)[M^{II}(H_2O)_6](SeO_4)_2$ (M^{II} = Ni (**I**) and M^{II} = Zn (**II**)) were grown from aqueous solutions of 1,4-diaza-bicyclo[2.2.2]octane, transition metals carbonate and selenic acid, with 1:1:2 M ratio. The reactants are dissolved in a minimum amount of distilled water. The clear solutions were stirred magnetically for 30 min and allowed to stand at room temperature. After a few days, green crystals of compound (**I**) and colorless crystals of compound (**II**) were isolated from the solutions. The chemical purity of the products was tested by EDAX measurements. Indeed, the EDAX spectra of compounds (**I**) and (**II**) reveal, respectively the presence of all non-hydrogen atoms: Ni or Zn, Se, O, N and C.

2.2. Single-crystal data collection and structure determination

A suitable crystal of $(C_6H_{14}N_2)[Ni(H_2O)_6](SeO_4)_2$ was glued to a glass fiber mounted on a four-circle Nonius Kappa CCD area-detector diffractometer. Intensity data sets were collected using MoKα radiation through the program COLLECT (Kappa CCD Program Software, 1998). Correction for Lorentz-polarisation effect, peak integration and background determination were carried out with the program DENZO (Otwinowski et al., 1997). Frame scaling and unit cell parameter refinement were performed with the program SCALEPACK (Otwinowski et al., 1997). Analytical absorption corrections were performed by modelling the crystal faces (De Meulenaer and Tompa, 1965).

For the zinc based compound $(C_6H_{14}N_2)[Zn(H_2O)_6](SeO_4)_2$, the XRD data were collected at room temperature by the ω-scan technique on an Oxford Diffraction supernova, dual, Cu at zero, four-circle diffractometer with an Atlas CCD-detector and graphite-monochromatized MoKα radiation. The data were corrected for Lorentz-polarization effects and an empirical absorption correction by Xabs2 (Parkin

Table 1 Crystallographic data for $(C_6H_{14}N_2)[M^{II}(H_2O)_6](SeO_4)_2$ (M^{II} = Ni (**I**) and M^{II} = Zn (**II**)).

Empirical formula	$(C_6H_{14}N_2)[Ni(H_2O)_6](SeO_4)_2$	$(C_6H_{14}N_2)[Zn(H_2O)_6](SeO_4)_2$
Formula weight (g/mol)	566.92	573.58
Crystal system	Monoclinic	Monoclinic
Space group	$P2_1/c$	$P2_1/c$
a (Å)	12.8366 (3)	12.7839 (2)
b (Å)	11.9360 (3)	11.9153 (4)
c (Å)	12.4045 (3)	12.3814 (2)
β (°)	108.518 (2)	108.264 (5)
V (Å^3)	1802.18 (8)	1790.97 (7)
Z	4	4
Crystal size (mm^3)	0.303∗0.420∗0.405	0.105∗0.088∗0.068
Color	Green	Colorless
Calculated density	2.089	2.127
λ (MoKα) (Å)	0.71073	0.71073
Absorption correction	Analytical Otwinowski et al. (1997)	Xabs2 De Meulenaer and Tompa (1965)
Measured reflections	23307	6547
Independent reflections	4111	6547
Reflections [$I > 2\sigma$ (**I**)]	3472	1805
Domain of θ (°)	3.25–27.44	3.25–32.97
T_{min} and T_{max}	0.37568–0.51300	0.599–0.717
Index ranges	$-15 \leqslant h \leqslant 16$	$-19 \leqslant h \leqslant 18$
	$-15 \leqslant k \leqslant 14$	$0 \leqslant k \leqslant 18$
	$-15 \leqslant l \leqslant 15$	$0 \leqslant l \leqslant 18$
Number of parameters	275	282
R_1	3.16%	2.01%
wR_2	7.89%	5.01%
GooF	0.980	1.088

et al., 1995) was performed. The structures analyses for both compounds were carried out with the monoclinic symmetry, space group $P2_1/c$, according to the automated search for the space group available in WinGX (Farrugia, 1999). Transition metal atoms (M^{II}) and selenium atoms were located using the direct methods with program SHELXS-97 (Sheldrick, 1997a). The oxygen atoms and the organic moieties were found from successive Fourier calculations using SHELXL-97 (Sheldrick, 1997b). The aqua H atoms were located in a different map and refined with O–H distance restraints of 0.85(2) Å and H...H restraints of 1.39(2) Å so that the H–O–H angle fitted to the theoretical value of 105.4°. H atoms bonded to C and N atoms were positioned geometrically and allowed to ride on their parent atoms, with C–H = 0.97 Å and N–H = 0.90 Å. Crystallographic data and structural refinements are summarized in Table 1. Bond distances and angles calculated from the final atomic coordinates, as well as probable hydrogen bonds, are listed in Table 2, respectively. The drawings were made with Diamond program (Brandenburg, 1998).

Further details of the crystal structure investigations can be obtained free of charge from the Cambridge Crystallographic Data Centre via www.ccdc.cam.ac.uk/data_request/cif. The deposition numbers are CCDC 903933 and CCDC 903934 for compounds (**I**) and (**II**), respectively.

2.3. Infrared spectroscopy

IR reflection spectrums of the title compounds were measured with a Perkin–Elmer BX FTIR spectrometer, in the 4000–400 cm^{-1} region at ambient temperature, with KBr pellets.

Table 2 Selected bond distances (Å) and angles (°).

Octahedron around $M^{II}(H_2O)_6$		Tetrahedron around Se(1)		Cation $(C_6H_{14}N_2)^{2+}$	
*$(C_6H_{14}N_2)[Ni(H_2O)_6](SeO_4)_2$ (**I**)*					
Ni–OW1	2.008 (2)	Se1–O1	1.629 (2)	N1–C1	1.491 (5)
Ni–OW2	2.026 (2)	Se1–O2	1.637 (2)	N1–C3	1.487 (4)
Ni–OW3	2.057 (2)	Se1–O3	1.638 (2)	N1–C5	1.499 (4)
Ni–OW4	2.054 (2)	Se1–O4	1.638 (2)	N2–C2	1.488 (5)
Ni–OW5	2.068 (3)	O1–Se1–O2	110.71 (15)	N2–C4	1.486 (5)
Ni–OW6	2.107 (2)	O1–Se1–O4	109.51 (13)	N2–C6	1.475 (4)
OW1–Ni–OW2	91.26 (11)	O2–Se1–O4	109.56 (12)	C1–C2	1.509 (5)
OW1–Ni–OW3	86.86 (11)	O1–Se1–O3	109.21 (14)	C3–C4	1.524 (5)
OW1–Ni–OW4	179.66 (10)	O2–Se1–O3	107.69 (12)	C5–C6	1.514 (5)
OW1–Ni–OW5	90.67 (11)	O4–Se1–O3	110.14 (13)	N1–C1–C2	108.6 (3)
OW1–Ni–OW6	92.02 (11)	Tetrahedron around Se(2)	N1–C3–C4	108.4 (3)	
OW2–Ni–OW3	176.96 (13)	Se2–O5	1.628 (2)	N1–C5–C6	107.6 (3)
OW2–Ni–OW4	88.92 (11)	Se2–O6	1.633 (2)	N2–C2–C1	109.0 (3)
OW2–Ni–OW5	88.57 (14)	Se2–O7	1.637 (2)	N2–C4–C3	108.6 (3)
OW2–Ni–OW6	89.17 (12)	Se2–O8	1.648 (2)	N2–C6–C5	109.8 (3)
OW3–Ni–OW5	93.84 (13)	O5–Se2–O6	110.57 (14)	C1–N1–C5	110.5 (3)
OW3–Ni–OW6	88.51 (11)	O5–Se2–O7	111.00 (14)	C2–N2–C4	109.2 (3)
OW4–Ni–OW3	92.95 (10)	O6–Se2–O7	109.10 (12)	C3–N1–C1	110.3 (3)
OW4–Ni–OW5	89.62 (11)	O5–Se2–O8	108.17 (13)	C3–N1–C5	110.1 (3)
OW4–Ni–OW6	87.69 (10)	O6–Se2–O8	109.75 (11)	C6–N2–C2	110.8 (3)
OW5–Ni–OW6	176.52 (11)	O7–Se2–O8	108.22 (12)	C6–N2–C4	110.5 (3)
*$(C_6H_{14}N_2)[Zn(H_2O)_6](SeO_4)_2$ (**II**)*					
Zn–OW1	2.1157 (11)	Se1–O1	1.6479 (10)	N1–C2	1.4936 (18)
Zn–OW2	2.0573 (11)	Se1–O2	1.6400 (10)	N1–C3	1.4928 (18)
Zn–OW3	2.1511 (10)	Se1–O3	1.6378 (9)	N1–C5	1.4932 (17)
Zn–OW4	2.0278 (10)	Se1–O4	1.6397 (10)	N2–C2	1.4928 (18)
Zn–OW5	2.0719 (10)	O1–Se1–O2	108.60 (5)	N2–C4	1.4880 (18)
Zn–OW6	2.0758 (10)	O1–Se1–O3	109.80 (5)	N2–C6	1.4949 (18)
OW1–Zn–OW2	88.73 (6)	O1–Se1–O4	108.15 (5)	C1–C2	1.530 (2)
OW1–Zn–OW3	175.57 (4)	O2–Se1–O3	108.84 (5)	C3–C4	1.524 (2)
OW1–Zn–OW4	90.98 (5)	O2–Se1–O4	111.02 (5)	C5–C6	1.529 (2)
OW1–Zn–OW5	88.94 (4)	O4–Se1–O3	110.40 (5)	N1–C2–C1	107.96 (11)
OW1–Zn–OW6	94.73 (5)	Tetrahedron around Se(2)	N1–C3–C4	108.30 (11)	
OW2–Zn–OW3	88.30 (5)	Se2–O5	1.6418 (10)	N1–C5–C6	108.74 (11)
OW2–Zn–OW4	90.75 (5)	Se2–O6	1.6440 (10)	N2–C1–C2	108.92 (12)
OW2–Zn–OW5	89.24 (4)	Se2–O7	1.6350 (10)	N2–C4–C3	109.08 (11)
OW2–Zn–OW6	175.70 (5)	Se2–O8	1.6389 (10)	N2–C6–C5	108.20 (11)
OW3–Zn–OW5	87.73 (4)	O5–Se2–O6	109.76 (5)	C2–N1–C5	109.82 (11)
OW3–Zn–OW6	88.39 (4)	O5–Se2–O7	109.41 (5)	C3–N1–C2	110.44 (11)
OW4–Zn–OW3	92.34 (4)	O5–Se2–O8	109.65 (5)	C3–N1–C5	110.12 (11)
OW4–Zn–OW5	179.92 (5)	O6–Se2–O7	109.42 (5)	C1–N2–C4	111.00 (12)
OW4–Zn–OW6	86.65 (4)	O6–Se2–O8	107.83 (5)	C6–N2–C1	109.43 (12)
OW5–Zn–OW6	93.36 (4)	O7–Se2–O8	110.75 (6)	C6–N2–C4	109.39 (12)

2.4. Thermal behavior

A thermogravimetric (TG) measurement was performed for compound (**I**) with a SETERAM TG-DTA92 instrument under flowing air, with a heating rate of 10 °C.min^{-1} from ambient temperature to 900 °C.

DTA/TG investigations for compound (**II**) were performed using a Perkin–Elmer Instruction system (STA6000) with a heating rate of 10 °C.min^{-1} under a nitrogen atmosphere.

2.5. Magnetic measurements

Magnetic susceptibility measurement in the range of 1.8–300 K was carried out on a powdered sample of the nickel based compound, at the magnetic field of 1000 Oe, using a Quantum Design SQUID Magnetometer (type MPMS-XL5).

3. Results and discussion

3.1. Description of the structures

Both supramolecular compounds $(C_6H_{14}N_2)[M^{II}(H_2O)_6](SeO_4)_2$ have similar crystalline structures and they crystallize at room temperature, in the monoclinic system, space group $P2_1/c$, with $Z = 4$. The crystal structure of these compounds consists of isolated divalent metals, M(II), octahedrally coordinated by six water molecules forming the $[M^{II}(H_2O)_6]^{2+}$ cations, selenate tetrahedra $(SeO_4)^{2-}$, and dabcodiium cations $(C_6H_{14}N_2)^{2+}$ linked together by hydrogen bond network only. As it can be seen in Figs. 1 and 2, the structures of the title compounds, can be described as an alternation, along the crystallographic *b* axis, of mixed cationic layers parallel to the (*a* and *c*) plane, formed by $[M^{II}(H_2O)_6]^{2+}$ octahedra and $(C_6H_{14}N_2)^{2+}$ cations, and anionic layers formed by the selenate groups. It is interesting to note here that the related sulfate phase containing nickel as the transition metal, $(C_6H_{14}N_2)[Ni(H_2O)_6](SO_4)_2$, presents a disorder of the dabcodiium cation which lies in special position on inversion center (Rekik et al., 2007). It can be concluded that the substitution of the sulfur atom by the selenium in this family of hybrid materials leads to a fully ordered structure in which the organic moieties occupy general positions.

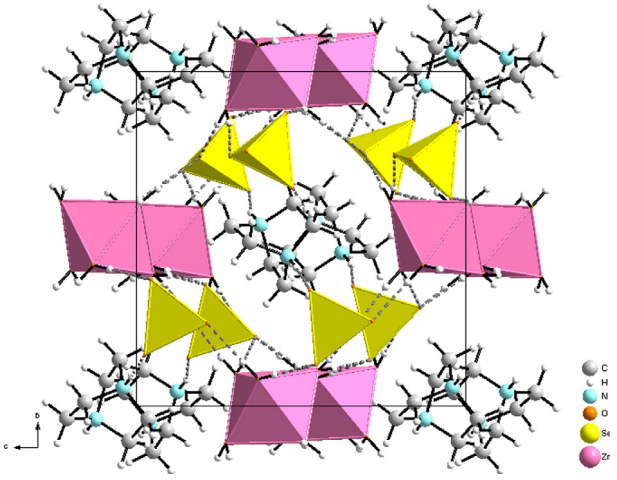

Figure 1 Projection of the crystal structure of compound (**II**) along the *a*-axis.

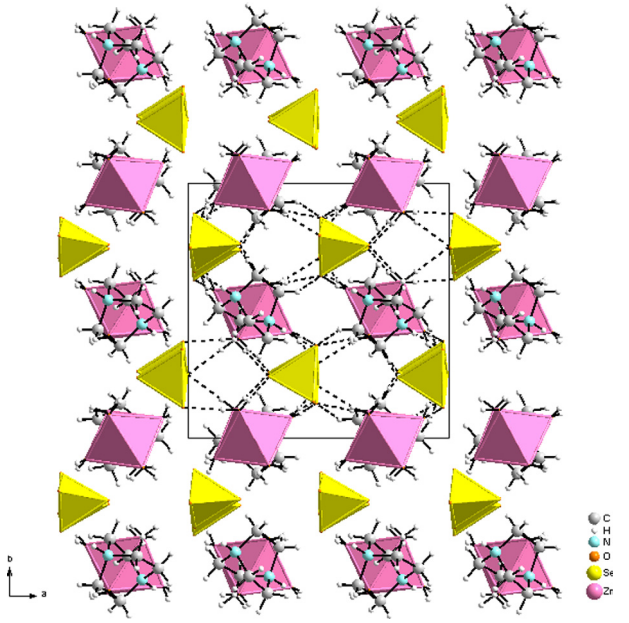

Figure 2 View of the structure of compound (**II**) along the *c*-axis. Hydrogen bonds are represented by dashed lines.

In these two compounds, the divalent metal occupies a general position and is located in the center of a slightly distorted octahedron formed by six water molecules. Within the metallic octahedron, the M^{II}–OW distances range from 2.008(2) to 2.107(2) Å and from 2.028(1) to 2.15(1) Å for the nickel and zinc compounds, respectively. The values of OW–M^{II}–OW angles are comprised between 86.86(11)° and 179.66(10)° in the Ni^{2+} octahedron and between 88.30(5)° and 179.92(5)° in the Zn^{2+} octahedron (Table 2). These geometric characteristics are consistent with those described in the literature for nickel (Rekik et al., 2007) and zinc (Yahyaoui et al., 2007) octahedron formed by six water molecules. The $M^{II}(H_2O)_6$ octahedra are separated from each other with shortest metal–metal distances of Ni–Ni = 6.1200(5) Å and Zn–Zn = 6.1027(3) Å. This difference observed in the intermetallic distances is certainly due to the size of the metallic cation involved in the structure; $r_{(Ni^{2+})} > r_{(Zn^{2+})}$. It should be noted that Ni–Ni distance in this hybrid material is shorter then that found in its analogue compound containing sulfate anion (Ni–Ni = 7.000(0) Å) (Rekik et al., 2007). This result is surprising because we expected a greater distance. Indeed the selenate anion is bigger than the sulfate tetrahedron, since the selenium atom is more voluminous than the sulfur atom. So that, the intermetallic distance depends not only on the entities involved in the structure but also on the structure type.

In both compounds, the metallic octahedra are arranged one above the other in a zigzag manner along the crystallographic *a*-axis (Fig. 1) and each of them is surrounded by seven selenate groups H-bonded, five in a bidentate manner and two in a monodentate fashion (Fig. 3). This result is different from that found in the $(C_6H_{14}N_2)[Ni(H_2O)_6](SO_4)_2$ compound where the octahedra run along the *a* and *c* axes, forming inorganic cationic stacks along [1 0 0] and [0 0 1] and each octahedron is H-bonded to six sulfate anions in a bidentate fashion (Rekik et al., 2007).

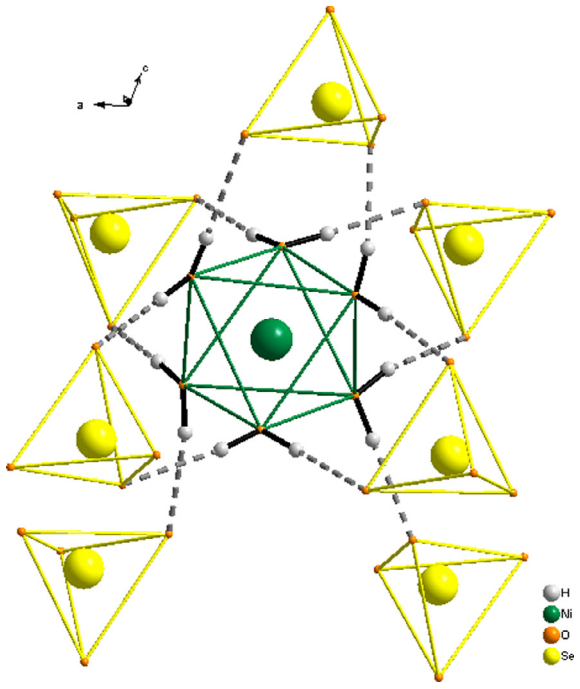

Figure 3 The environment around the metal atom and the hydrogen bonds established between $Ni(H_2O)_6$ and SeO_4 in compound (**I**).

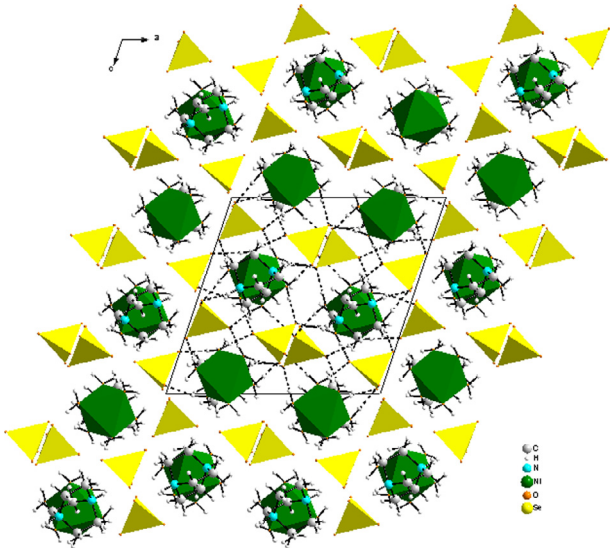

Figure 4 Projection of the crystal structure for compound (**I**) along the *b*-axis.

The organic cations, $(C_6H_{14}N_2)^{2+}$, are also located in general position and they occupy the same positions of the metallic octahedra translated by half of the *b* axis. Then, they run along the *a* axis to form organic cationic stacks along [1 0 0] (Fig. 1) and they alternate with $[M^{II}(H_2O)_6]^{2+}$ cations along the *c* (Fig. 2) and *b*-axis (Fig. 4) to form mixed cationic layers parallels to the (a and c) plane. It is important to note that there is no connection between the two types of cations.

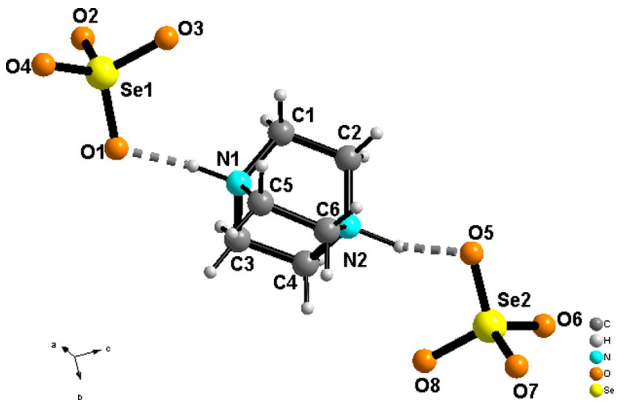

Figure 5 Hydrogen bonds formed between $(C_6H_{14}N_2)^{2+}$ and SeO_4 tetrahedra in compound (**I**).

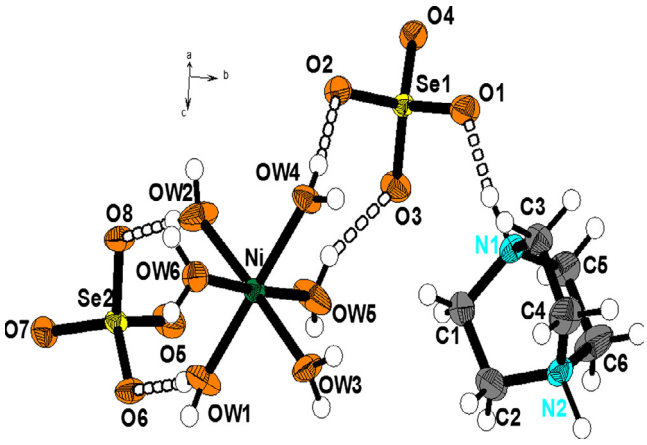

Figure 6 A part of the crystal structure of compound (**I**), showing the asymmetric unit and atom numbering**.** Displacement ellipsoids are drawn at the 50% probability level. Hydrogen bonds are represented by dashed lines.

Indeed, the protonated diamines are linked only to the selenate tetrahedra via hydrogen N–H...O bonds (Fig. 5). The characteristic bond distances and angles within the protonated diamine molecule, listed in Table 2, are in agreement with those observed in other compounds containing the same groups (Rekik et al., 2006b, 2007).

Within the asymmetric unit of each compound (Fig. 6), there are two crystallographically distinct Se atoms with tetrahedral coordination geometry. The SeO_4 tetrahedra are slightly distorted. The geometric characteristics of the SeO_4 tetrahedron are given in Table 2. The Se–O distances and O–Se–O angles do not present any particularity and they are comparable to those observed in other compounds containing the same group. The quite regular selenate groups are located between the mixed cationic layers forming anionic pseudo-layers parallel to the (a and c) plane. Then cationic and anionic layers alternate along the *b* axis in the *ABAB*... fashion and are held together by N–H...O and OW–H...O hydrogen bonds (Figs. 1 and 2). Within the intermolecular hydrogen bonds **D–H...A, the Donor...Acceptor distances values range from 2.652(4) to 2.962(3) Å and between 2.6445(15) and

Table 3 Hydrogen-bonding geometry (Å, °).

	D–H (Å)	H...A (Å)	D...A (Å)	D–H...A (°)
*$(C_6H_{14}N_2)[Ni(H_2O)_6](SeO_4)_2$ (**I**)*				
N1–HN1–O1	0.91	1.77	2.666 (4)	169.0
N2–HN2–O5 ^{I}	0.91	1.81	2.680 (4)	158.1
OW1–H11–O7 ^{II}	0.833 (18)	1.906 (19)	2.732 (3)	171 (4)
OW1–H12–O6	0.829 (18)	1.89 (2)	2.712 (3)	172 (4)
OW2–H21–O8	0.837 (19)	1.903 (19)	2.735(3)	173 (5)
OW2–H22–O2 ^{III}	0.849 (19)	1.82 (2)	2.652 (4)	165 (5)
OW3–H31–O6 ^{IV}	0.866 (18)	1.91 (2)	2.768 (3)	170 (4)
OW3–H32–O3 ^{I}	0.859 (18)	1.89 (2)	2.733 (3)	168 (4)
OW4–H41–O4 ^{I}	0.855 (18)	1.938 (19)	2.791 (3)	176 (3)
OW4–H42–O2	0.861 (18)	1.841 (18)	2.701 (3)	177 (4)
OW5–H51–O3	0.837 (18)	2.04 (3)	2.831 (4)	158 (4)
OW5–H52–O7 ^{V}	0.835 (18)	1.882 (18)	2.716 (4)	177 (4)
OW6–H61–O4 ^{III}	0.845 (19)	2.123 (19)	2.962 (3)	172 (5)
OW6–H62–O8 ^{II}	0.850 (19)	2.02 (2)	2.861 (3)	171 (5)
Symmetry codes: $^{I}x, -y + 3/2, z-1/2$, $^{II}x, -y + 1/2, z-1/2$, $^{III}-x, -y + 1, -z$, $^{IV}1-x, 1-y, -z$, $^{V}1-x, y + 1/2, -z + 1/2$				
*$(C_6H_{14}N_2)[Zn(H_2O)_6](SeO_4)_2$ (**II**)*				
N1–HN1–O7	0.83 (2)	1.82 (2)	2.6519 (15)	173 (2)
N2–HN2–O4^{I}	0.97 (2)	1.71 (2)	2.6487 (15)	163 (2)
OW1–H11–O2^{II}	0.833 (15)	1.889 (15)	2.7167 (15)	172 (2)
OW1–H12–O6^{III}	0.826 (14)	1.984 (15)	2.7995 (15)	170 (2)
OW2–H21–O1^{III}	0.798 (15)	1.918 (15)	2.7152 (15)	178 (2)
OW2–H22–O8^{IV}	0.815(15)	1.851(15)	2.6445(15)	164(2)
OW3–H31–O1	0.834 (15)	1.990 (15)	2.8233 (14)	180 (2)
OW3–H32–O5^{IV}	0.833 (15)	2.071 (15)	2.8986 (14)	172 (2)
OW4–H41–O3^{III}	0.821 (15)	1.883 (15)	2.7015 (14)	175 (2)
OW4–H42–O2	0.808 (15)	1.911 (15)	2.7164 (14)	175 (2)
OW5–H51–O5^{V}	0.823 (14)	1.947 (15)	2.7607 (14)	170 (2)
OW5–H52–O8^{III}	0.808 (15)	1.889 (15)	2.6948 (14)	176 (2)
OW6–H61–O3^{VI}	0.854 (14)	1.905 (15)	2.7512 (14)	171 (2)
OW6–H62–O6^{V}	0.858 (15)	1.849 (15)	2.7023 (14)	173 (2)
Symmetry codes: $^{I}x, 3/2-y, -1/2 + z$; $^{II}1-x, -y, 1-z$; $^{III}x, 1/2-y, 1/2 + z$; $^{IV}-x, -1/2 + y, 1/2-z$; $^{V}x, -1 + y, z$; $^{VI}1-x, -1/2 + y, 1/2-z$				

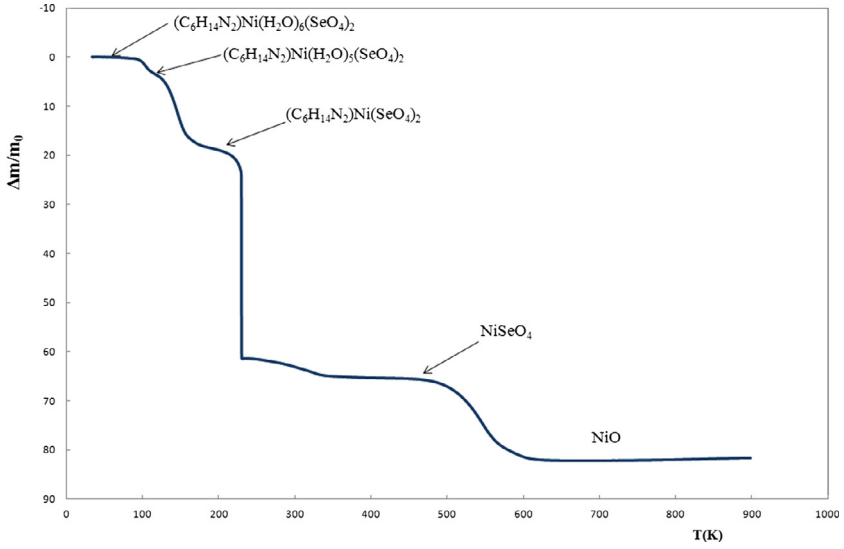

Figure 7 TG curve for the decomposition of $(C_6H_{14}N_2)[Ni(H_2O)_6](SeO_4)_2$ in air (10 °C min^{-1}).

2.8986(14) Å in the nickel and zinc compounds, respectively (Table 3).

It is important to note that the structure can be also described as corrugated layers with an average plane (400). These layers are stabilized and interconnected by hydrogen bonds (Fig. 2).

3.2. Infrared spectroscopy

*3.2.1. Nickel compound (**I**)*

The IR spectrum of the nickel-based compound shows characteristic absorption bands at 414 and 878 cm^{-1} due to the

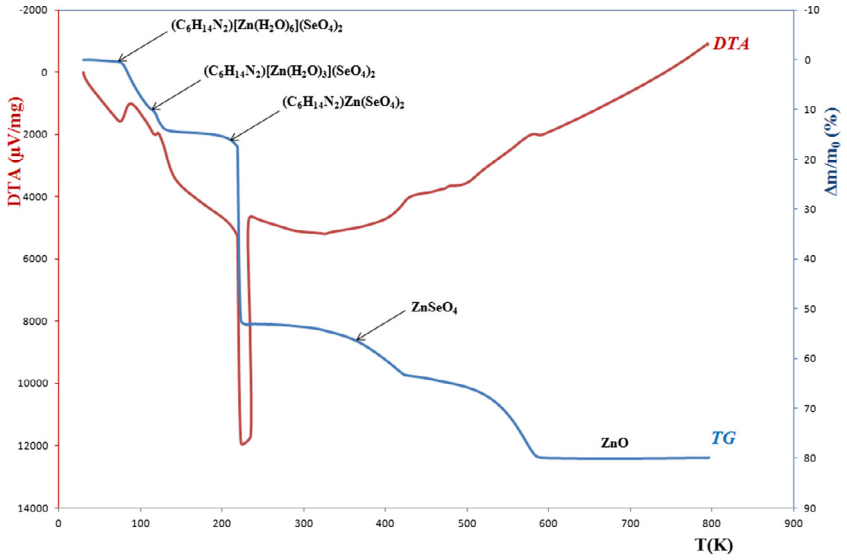

Figure 8 DTA-TG curves for the decomposition of $(C_6H_{14}N_2)[Zn(H_2O)_6](SeO_4)_2$ in air (10 °C min^{-1}).

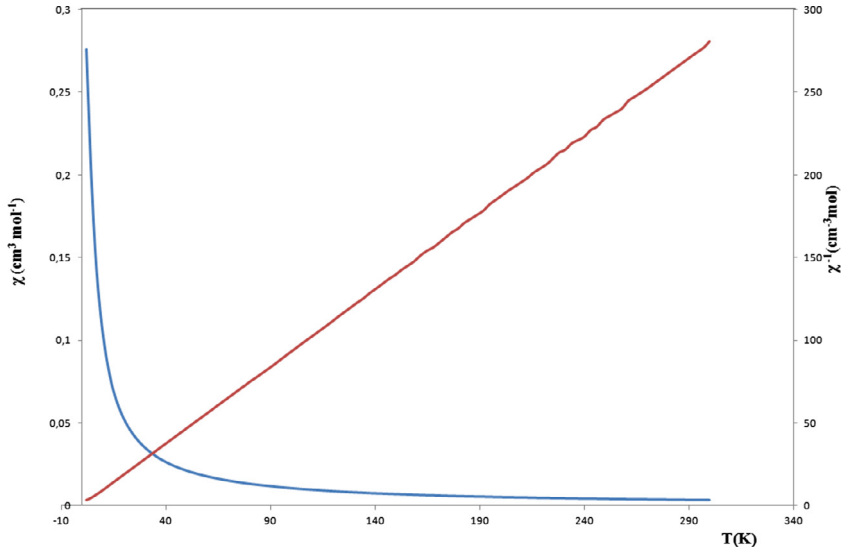

Figure 9 Temperature dependencies of the magnetic susceptibility and its inverse in the temperature range 1.8–300 K.

asymmetry bending and symmetry stretching vibrations of the SeO_4 group, respectively. The bending and stretching vibrations of water molecules are appeared as a band at 1672 cm^{-1} and a broad band at 3207 cm^{-1}, respectively. The other spectrum bands are assigned to the amine in its protonation form: the broad peak which appears at 2616 cm^{-1} is due to the bending vibrations of the $-NH^+$ group. The intense band situated at 1320 cm^{-1} can be assigned to the bending vibrations out of plane (wagging or twisting) of the CH_2 group. Three other peaks at 1471, 1437 and 1412 cm^{-1} indicate the bending vibrations (scissoring) of the CH_2 group. In addition, the band at 2804 cm^{-1} is due to the stretching vibrations of CH_2. A sharp peak at 1054 cm^{-1} is due to the vibrations of skeletal motion of the amine (dabco).

3.2.2. Zinc compound (*II*)

The presence of the template is confirmed by the IR spectroscopy with the $-NH^+$ group measured at 2197 cm^{-1} due to the bending vibrations. The stretching vibrations of the CH_2 group are observed at 3022 and 3239 cm^{-1}. The sharp peaks at 702 and 1059 cm^{-1} are due to the vibrations of skeletal motion of the amine (dabco). Se–O bands are observed at 491 and 822 cm^{-1} due to the asymmetry bending and symmetry stretching vibrations, respectively. The bending and stretching vibrations of water molecules appeared as a band at 1616 cm^{-1} and a broad band at 3853 cm^{-1}, respectively.

3.3. Thermal decomposition

3.3.1. Nickel compound (*I*)

The thermogravimetry curve obtained during the decomposition of $(C_6H_{14}N_2)[Ni(H_2O)_6](SeO_4)_2$ under flowing air is shown in Fig. 7. The thermal decomposition of compound (**I**) takes place in several steps. In the first stage, the supramolecular compound looses one water molecule in the temperature range 96–120 °C (observed weight loss, 3.76%; calculated weight loss, 3.15%). The second step of the decomposition (temperature range 124–170 °C) corresponds to the full dehydration of the

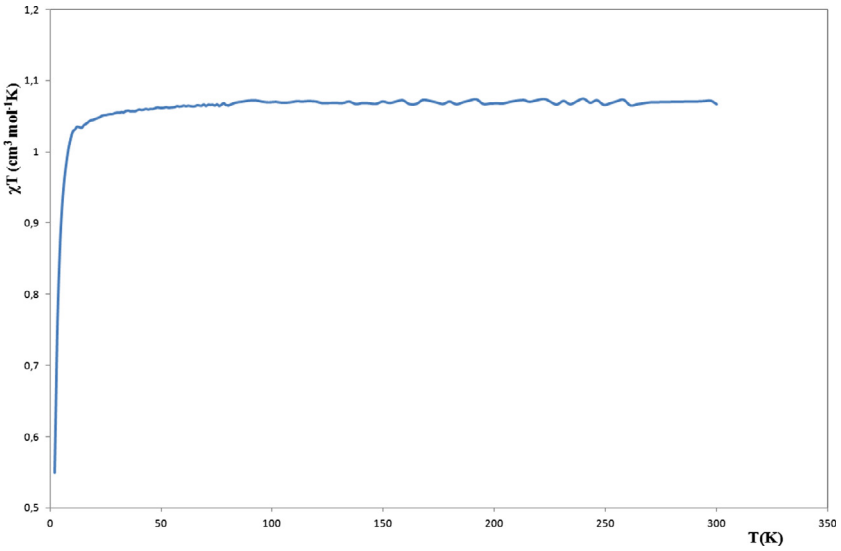

Figure 10 χ.T evolution versus temperature for $(C_6H_{14}N_2)[Ni(H_2O)_6](SeO_4)_2$.

compound by the loss of five water molecules (observed weight loss, 17.45%; calculated weight loss, 15.83%) thus leading to the anhydrous phase, $(C_6H_{14}N_2)Ni(SeO_4)_2$. This result is different from that found in the $(C_6H_{14}N_2)[Ni(H_2O)_6](SO_4)_2$ compound where the dehydration occurs in only one step by the departure of six water molecules (Rekik et al., 2007). The anhydrous phase, $(C_6H_{14}N_2)Ni(SeO_4)_2$, is not stable and decomposes into $NiSeO_4$ (observed weight loss, 57.24%; calculated weight loss, 54.63%). The last transformation corresponds to the formation of nickel oxide, NiO (observed weight loss 75.38%, calculated weight loss 77.5%).

*3.3.2. Zinc compound (**II**)*

The thermogravimetry (TG) and differential thermal analysis (DTA) curves obtained during the decomposition of compound (**II**) are given in Fig. 8. They demonstrate that the decomposition of the precursor is complex and takes place through several stages giving rise to the zinc oxide. The rapid weight loss (10.025%) observed on TG curve between ambient temperature and 125 °C is attributed to the departure of the three less linked water molecules (calculated weight loss, 9.418%). This phenomenon is accompanied with a weak endothermic peak on the DTA curve. The second weight loss of 16.07%, observed between 130 and 222 °C on TG curve and accompanied with an intense endothermic peak, corresponds to the full dehydration of the precursor giving rise to an anhydrous phase. Theoretical, the departure of six water molecules corresponds to the weight loss of 18.83%. The next step corresponds to the decomposition of the anhydrous phase. It is indicated on the DTA curve by two endothermic medium peaks. The departure of the amine selenate $(C_6H_{14}N_2)(SeO_4)$ appears on the TG curve (observed weight loss, 56.48%; calculated weight loss, 55.17%). The last stage corresponding to the transformation of the zinc selenate into the zinc oxide (calculated weight loss, 77.85%).

3.4. Magnetic properties

Magnetic susceptibilities were measured using a SQUID magnetometer (type MPMS-XL5), in the temperature range 1.8–300 K. After zero cooling and stabilization of the temperature at 300 K, a magnetic field of 1000 Oe was applied. The magnetic susceptibilities were measured with decreasing the temperature to 1.8 K. Fig. 9 represents the magnetic susceptibility and its inverse evolutions versus temperature for $(C_6H_{14}N_2)[Ni(H_2O)_6](SeO_4)_2$. It shows that susceptibility values follow a Curie–Weiss law $\chi_m = C/(T-\theta)$ from room temperature to 22 K with $C = 1.08\ cm^3\ mol^{-1}\ K$ and $\theta = -2$ K close to expected $S = 1$, where χ_m is the molar magnetic susceptibility of nickel(II) ion and C and θ are the Curie and Weiss constants, respectively. These values indicate that the compound is predominantly paramagnetic with weak antiferromagnetic interactions. The thermal dependence of $\chi_m.T$ appears in Fig. 10. Parameter C obtained from the linear fit of $1/\chi$ (T) curve (Fig. 9) was used for the calculation of the effective magnetic moment per nickel(II) atom according to expression $\mu_{eff} = (8C)^{1/2}\mu_B$ (Smart, 1963) giving $\mu_{eff} = 2.93\ \mu_B$. This value corresponds to two unpaired electrons per formula unit. The expected value of the effective magnetic moment for the spin-only of uncoupled Ni(II) metal ion is $\mu_{eff} = 2[S(S+1)]^{1/2} = 2.828\ \mu_B$ with $S = 1$.

4. Concluding remarks

In this work, two new isostructural divalent metal selenates templated by 1,4-diaza-bicyclo[2.2.2]octane with general formula $(C_6H_{14}N_2)[M^{II}(H_2O)_6](SeO_4)_2$, M^{II} = Ni or Zn, have been synthesized. Their crystal structure consists of isolated entities linked by hydrogen bonds only, namely, two selenate groups playing the role of anions, $(C_6H_{14}N_2)^{2+}$ and bivalent transition metal surrounded by six water molecules, $[M^{II}(H_2O)_6]^{2+}$, playing the role of cations. The thermal decomposition of both the compounds proceeds through several stages giving rise to the respective metal oxide. The Magnetic measurements indicate that the nickel double selenate templated by dabco is paramagnetic in the temperature range 22–300 K with weak antiferromagnetic interactions at lower temperature.

Acknowledgement

Grateful thanks are expressed to Dr. T. Roisnel (Centre de Diffractométrie X, Université de Rennes I) and Dr. S. Dahaoui (CRM2; Université de Nancy) for their assistance in single-crystal X-ray diffraction data collection for compounds (**I**) and (**II**), respectively.

Appendix A. Supplementary data

Supplementary data associated with this article can be found, in the online version, at http://dx.doi.org/10.1016/j.arabjc.2013.09.019.

References

Borkowski, L.A., Cahill, C.L., 2006. Cryst. Growth Des. 6 (10), 2248–2259.
Brandenburg, K., 1998. Diamond version 2.0 Impact GbR, Bonn Germany.
Cheetham, A.K., Férey, G., Loiseau, T., 1999. Angew. Chem. Int. Ed. 38, 3268.
De Meulenaer, J., Tompa, H., 1965. Acta Crystallogr. 19, 1014.
Doran, M.B., Norquist, A.J., O'Hare, D., 2003. Inorg. Chem. 42 (22), 6989–6995.
Doran, M.B., Norquist, A.J., Stuart, C.L., O'Hare, D., 2004. Acta Crystallogr. E 60, M996–M998.
Doran, M.B., Norquist, A.J., O'Hare, D., 2005. Acta Crystallogr. E 61, M881–M884.
Farrugia, L.J., 1999. J. Appl. Crystallogr. 32, 837.
Feng, Mei-Ling, Mao, Jiang-Gao, Song, Jun-Ling, 2004. J. Solid State Chem. 177, 3529.
Feng, Mei-Ling, Ye, Heng-Yun, Mao, Jiang-Gao, 2007. J. Solid State Chem. 180, 2471–2477.
Férey, G., 2001. Chem. Mater. 13, 3084.
Finn, R., Zubieta, J., 2000. Chem. Commun., 1321.
Frisch, M., Cahill, C.L., 2007. J. Solid State Chem. 180 (9), 2597–2602.
Grechishnikova, E.V., Virovets, A.V., Peresypkina, E.V., Serezhkina, L.B., 2006. Russ. J. Coord. Chem. 32 (8), 586–589.
Hagrman, P.J., Hagrman, D., Zubieta, J., 1999. Angew. Chem. Int. Ed. 38, 2638.
Nonius, 1998. Kappa CCD Program Software. Nonius BV, Delft, Newyork.
Knope, K.E., Cahill, C.L., 2007. Inorg. Chem. 46 (16), 6607–6612.
Krivovichev, S.V., Kahlenberg, V., Avdontseva, E.Y., Mersdorf, E., Kaindl, R., 2005a. Eur. J. Inorg. Chem. 9, 1653–1656.
Krivovichev, S.V., Tananaev, I.G., Kahlenberg, V., Myasoedov, B.F., 2005b. Dokl. Phys. Chem. 403, 124–127.
Krivovichev, S.V., Tananaev, I.G., Myasoedov, B.F., 2007. C. R. Chim. 10 (10–11), 890–897.
Ling, Jie, Sigmon, Ginger E., Burns, Peter C., 2009. J. Solid State Chem. 182, 402–408.
Maslen, E.N., Ridout, S.C., Watson, K.J., Moore, F.H., 1988. Acta Cryst. C44, 409–412.
Naïli, H., Rekik, W., Bataille, T., Mhiri, T., 2006. Polyhedron 25, 3543.
Norquist, A.J., Doran, M.B., Thomas, P.M., O'Hare, D., 2003. Inorg. Chem. 42 (19), 5949–5953.
Norquist, A.J., Doran, M.B., O'Hare, D., 2005a. Inorg. Chem. 44 (11), 3837–3843.
Norquist, A.J., Doran, M.B., O'Hare, D., 2005b. Acta Crystallogr. E 61, M807–M810.
Ok, K.M., O'Hare, D., 2007. J. Solid State Chem. 180 (2), 446–452.
Ok, K.M., Doran, M.B., O'Hare, D., 2006. J. Mater. Chem. 16 (33), 3366–3368.
Otwinowski, Z., Minor, W., Carter, C.W., Sweet, R.M., 1997. In: Methods in Enzymology, vol. 276. Academic Press, Newyork, 307.
Parkin, S., Moezzi, B., Hope, H., 1995. J. Appl. Crystallogr. 28, 53.
Pasha, Intyaj, Choudhury, Amitava, Rao, C.N.R., 2003. J. Solid State Chem. 174, 386.
Rekik, W., Naïli, H., Mhiri, T., Bataille, T., 2005. Acta Cryst. E66, m629.
Rekik, W., Naïli, H., Bataille, T., Roisnel, T., Mhiri, T., 2006a. Inorg. Chim. Acta 359, 3954.
Rekik, W., Naïli, H., Bataille, T., Mhiri, T., 2006b. J. Organomet. Chem. 691, 4725–4732.
Rekik, W., Naïli, H., Mhiri, T., Bataille, T., 2007. J. Chem. Cryst. 37, 147.
Rekik, W., Naïli, H., Mhiri, T., Bataille, T., 2009. Acta Cryst. E65, m1404–m1405.
Rekik, W., Naïli, H., Mhiri, T., Bataille, T., 2009. Solid State Sci. 11, 614–621.
Sheldrick, G.M., 1997a. SHELXS-97, Program for Crystal Structure Solution. University of Göttingen, Germany.
Sheldrick, G.M., 1997b. SHELXL-97, Program for Crystal Structure Refinement. University of Göttingen, Germany.
Smart, J.S., 1963. In: Rado, G.T., Shul, H. (Eds.), . In: Magnetism, vol. 3. Academic Press, New York, p. 63.
Soghomonian, V., Chen, Q., Haushalter, R.C., Zubieta, J., Oconner, C.J., 1993. Science 259, 1596.
Wang, C.M., Liao, C.H., Lin, H.M., Lii, K.H., 2004. Inorg. Chem. 43 (26), 8239–8241.
Yahyaoui, S., Rekik, W., Naïli, H., Mhiri, T., Bataille, T., 2007. J. Solid State Chem. 180, 3560–3570.
Yu, Z.T., Liao, Z.L., Jiang, Y.S., Li, G.H., Li, G.D., Chen, J.S., 2004. Chem. Commun. 16, 1814–1815.
Zhang, W., Chen, L., Xiong, R., Nakamura, T., Huang, S.D., 2009. J. Am. Chem. Soc. 131, 12544–12545.